UC Santa Cruz
UC Santa Cruz Previously Published Works

Title

An integrated design and fabrication strategy for entirely soft, autonomous robots.

Permalink

Journal

ISSN

Authors

Wehner, Michael
Truby, Ryan L
Fitzgerald, Daniel J
et al.

Publication Date

DOI

Supplemental Material

Peer reviewed

LETTER

An integrated design and fabrication strategy for entirely soft, autonomous robots

Michael Wehner[1,2]*, Ryan L. Truby[1,2]*, Daniel J. Fitzgerald[1,2], Bobak Mosadegh[3,4], George M. Whitesides[2,5], Jennifer A. Lewis[1,2] & Robert J. Wood[1,2]

Soft robots possess many attributes that are difficult, if not impossible, to achieve with conventional robots composed of rigid materials[1,2]. Yet, despite recent advances, soft robots must still be tethered to hard robotic control systems and power sources[3–10]. New strategies for creating completely soft robots, including soft analogues of these crucial components, are needed to realize their full potential. Here we report the untethered operation of a robot composed solely of soft materials. The robot is controlled with microfluidic logic[11] that autonomously regulates fluid flow and, hence, catalytic decomposition of an on-board monopropellant fuel supply. Gas generated from the fuel decomposition inflates fluidic networks downstream of the reaction sites, resulting in actuation[12]. The body and microfluidic logic of the robot are fabricated using moulding and soft lithography, respectively, and the pneumatic actuator networks, on-board fuel reservoirs and catalytic reaction chambers needed for movement are patterned within the body via a multi-material, embedded 3D printing technique[13,14]. The fluidic and elastomeric architectures required for function span several orders of magnitude from the microscale to the macroscale. Our integrated design and rapid fabrication approach enables the programmable assembly of multiple materials within this architecture, laying the foundation for completely soft, autonomous robots.

Soft robotics is a nascent field that aims to provide safer, more robust robots that interact with humans and adapt to natural environments better than do their rigid counterparts. Unlike conventional robots composed of rigid materials, soft robots based on hydrogels[15,16], electroactive polymers[17], granular media[18] and elastomers[5,19] exhibit elastic moduli ranging from 10 kPa to 1 GPa (ref. 1), are physically resilient[7,20] and have the ability to passively adapt to their environment[1,2,19]. Moulded and laminated elastomers with embedded pneumatic networks are widely used materials in soft robotics[1,21,22]. Actuation of these elastomeric composites occurs when interconnected channels that make up the pneumatic network are inflated with incompressible fluids or gases supplied via tethered pressure sources[1]. Robotic end effectors with bioinspired[10] and rapid[6] actuation, deployable crawlers[3,7] and swimmers[8] with complex body motions, and robust jumpers[9,23] have been developed on the basis of this design strategy. However, in each case, these robots are either tethered to or carry rigid systems for power and control, yielding hybrid soft–rigid systems[4,7–9].

Creating a new class of fully soft, autonomous robots[24] is a grand challenge, because it requires soft analogues of the control and power hardware currently used. Recently, monopropellant fuels have been suggested as a promising fuel source for pneumatically actuated soft robots[4,12]. Their rapid decomposition into gas upon exposure to a catalyst offers a strategy for powering soft robotic systems that obviates the need for batteries or external power sources. Here, we report a method for creating a completely soft, pneumatic robot—the 'octobot'—with eight arms that are powered by monopropellant decomposition.
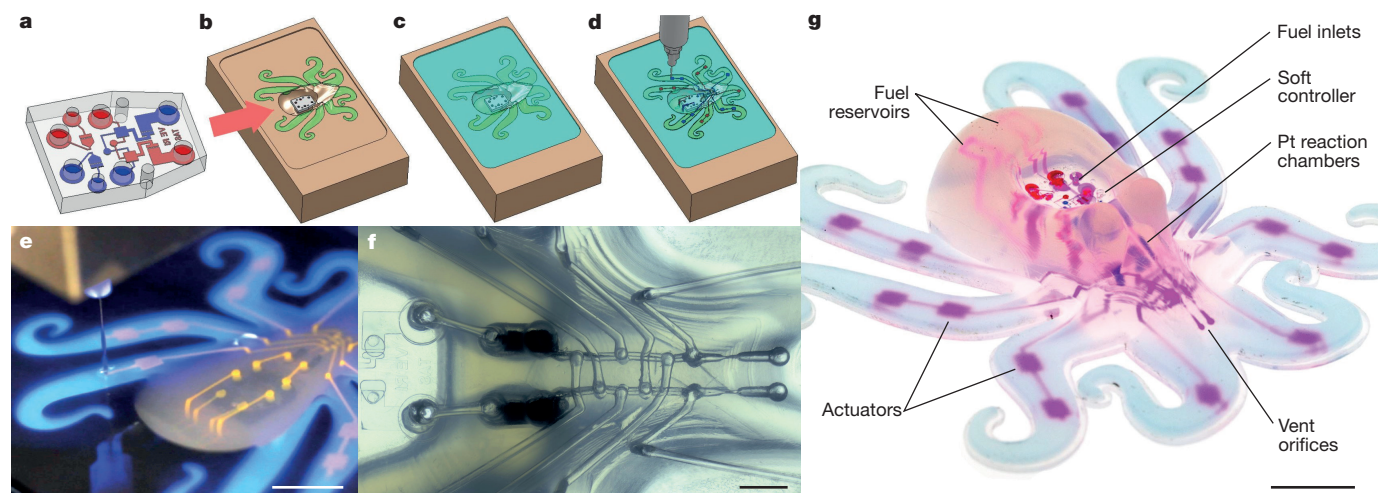

Figure 1 | Fully soft, autonomous robot assembly. a, b, A microfluidic soft controller is pre-fabricated (**a**) and loaded into a mould (**b**). **c–e,** Matrix materials are poured into the mould (**c**) and fugitive and catalytic inks are EMB3D printed (**d, e**). Scale bar in **e**, 10 mm. **f,** After matrix curing, the printed fugitive inks auto-evacuate, yielding open channels. Scale bar, 2 mm. **g,** The octobot is removed from the mould and inverted to reveal a fully soft, autonomous robot that is controlled via the embedded microfluidic soft controller and powered by monopropellant decomposition. Scale bar, 10 mm. Fluorescent dyes have been added in **e** and **g** to assist in visualization of internal features.

[1]John A. Paulson School of Engineering and Applied Sciences, Harvard University, Cambridge, Massachusetts 02138, USA. [2]Wyss Institute for Biologically Inspired Engineering, Harvard University, Cambridge, Massachusetts 02138, USA. [3]Dalio Institute of Cardiovascular Imaging, Weill Cornell Medicine and New York Presbyterian Hospital, New York, New York 10021, USA. [4]Department of Radiology, Weill Cornell Medicine, New York, New York 10021, USA. [5]Department of Chemistry and Chemical Biology, Harvard University, Cambridge, Massachusetts 02138, USA.
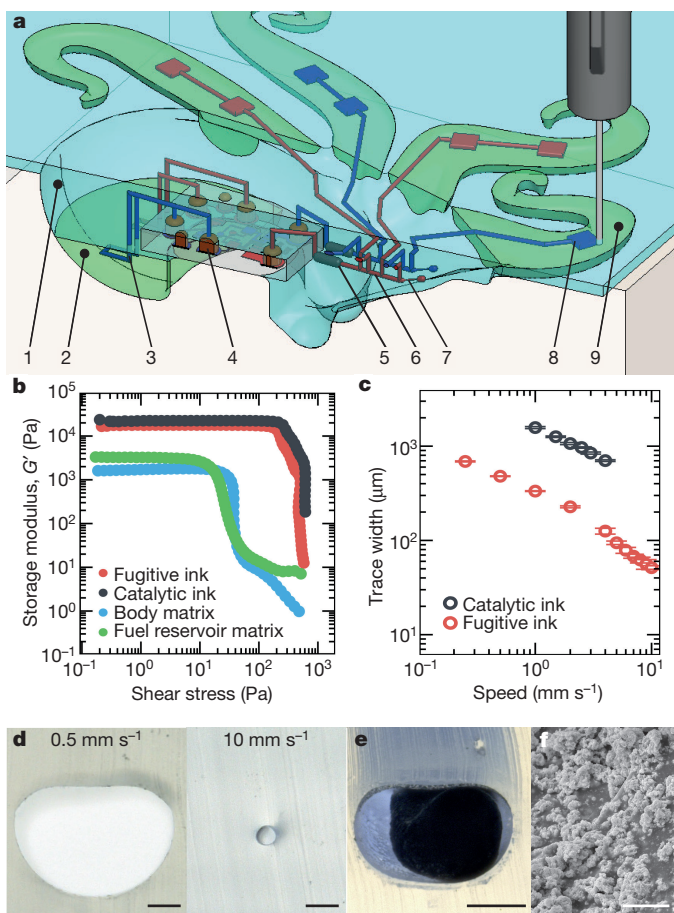*These authors contributed equally to this work.

Figure 2 | Multi-material, EMB3D printing. a, The octobot features include (1) the body matrix, (2) the fuel reservoir matrix, (3) printed fuel reservoir traces, (4) fugitive plugs in the soft controller, (5) printed platinum reaction chambers, (6) printed pneumatic networks, (7) printed vent orifices, (8) printed actuators and (9) moulded hyperelastic actuator matrix. All printed features are composed of the fugitive ink except the printed platinum reaction chambers (5), which are patterned using the catalytic ink. **b**, The storage modulus, G', of the fugitive ink, catalytic ink, body matrix and fuel reservoir matrix as a function of shear stress. The plateau moduli of the inks are an order of magnitude higher than those of the matrix materials. **c**, Trace widths of the fugitive and catalytic inks printed at 450 kPa and 345 kPa, respectively, decrease with print speed. Error bars indicate the standard deviation for $n = 3$ measurements. **d**, Optical images of channel cross-sections printed at speeds of 0.5 mm s^{-1} and 10 mm s^{-1}, which demonstrate that trace dimensions can be changed on-the-fly. Scale bars, 100 μm. **e**, **f**, Reaction chambers printed with the catalytic inks contain a platinum-laden plug, as shown in a cross-section (**e**; scale bar, 500 μm) and a scanning electron micrograph (**f**; scale bar, 25 μm).

To accomplish this, we use microfluidic logic[11] as a soft controller and a multi-material, embedded 3D (EMB3D) printing method to fabricate pneumatic networks within a moulded, elastomeric robot body. Our hybrid assembly approach allows one to seamlessly integrate soft lithography, moulding and 3D printing to rapidly and programmably fabricate a range of materials and functional elements in the form factors that are required for autonomous, untethered operation of a soft robot.

To fabricate an octobot, we first micro-mould[11,25] the soft controller that houses the microfluidic logic necessary for controlling fuel decomposition (Fig. 1a). The soft controller, which is protected temporarily with a polyimide mask, is placed into a mould that is partially filled by hyperelastic layers, which are needed for actuation (Fig. 1b). Matrix materials are then poured into the mould (Fig. 1c) and the remaining soft robot features are EMB3D printed into the moulded matrix (Fig. 1d, e, Supplementary Video 1). After the matrix materials are cross-linked, the aqueous inks 'auto-evacuate' at elevated temperature
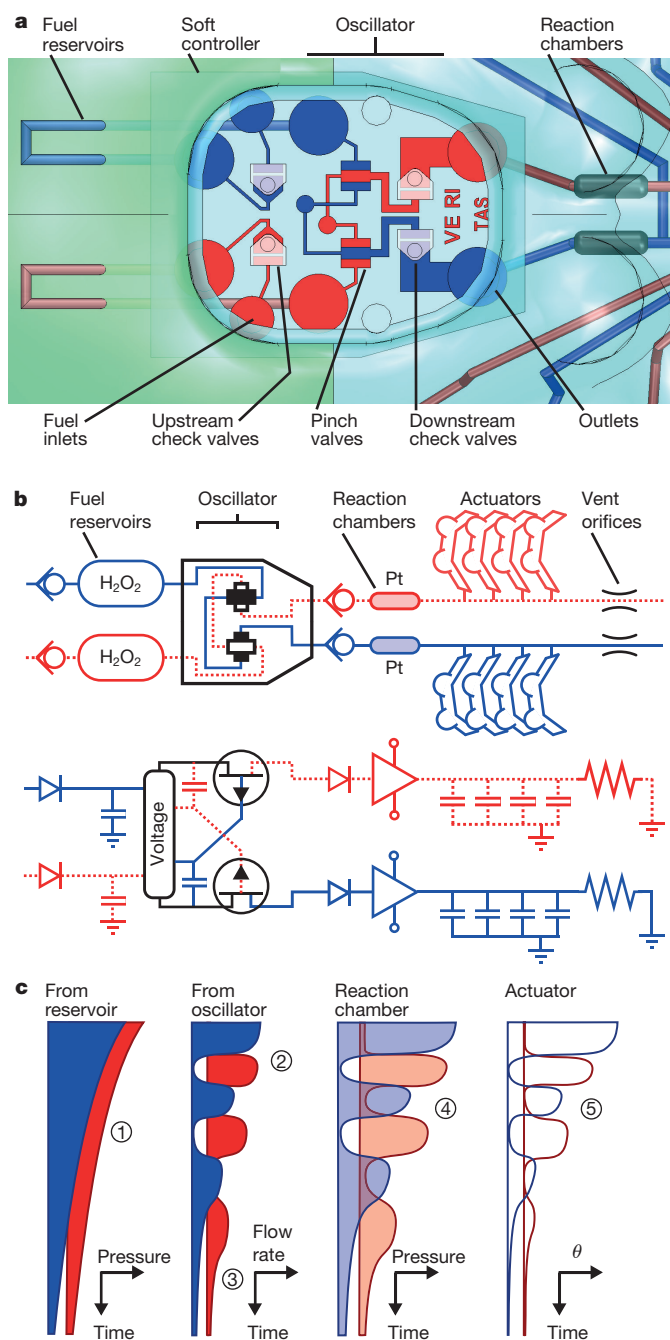

Figure 3 | Octobot control logic. Discrete sides are shown in red and blue for clarity. **a**, A system of check valves and switch valves within the soft controller regulates fluid flow into and through the system. The letters of 'VERITAS', each with a height of 500 μm, are patterned into the soft controller as an indication of scale. **b**, A schematic (top) and qualitative electrical analogy (bottom) of the octobot system; check valves, fuel tanks, oscillator, reaction chambers, actuators and vent orifices are akin to diodes, supply capacitors, electrical oscillator, amplifiers, capacitors and pull-down resistors, respectively. **c**, Conceptual curves show key variables as a function of time. (1) Nominal pressure drives fuel through system at a decreasing rate. (2) Pinch valves in the oscillator convert upstream flow into alternating flow between red and blue channels. Flow rate and switching frequency are functions of upstream pressure and downstream impedance. (3) When upstream pressure is too low, oscillation is not possible, so both sides flow at a reduced rate. (4) Catalyst decomposes fuel, yielding pressurized gas, which flows downstream to the actuators and the vent orifices concurrently. (5) Actuators deform (θ, actuator tip angle) as the pressure changes. Vents must be sufficiently small to allow full actuation, yet sufficiently large to allow timely venting.

as water evaporates and diffuses through the matrix, leaving behind an open network of channels that are interfaced with the soft controller (Fig. 1f). Octobot fabrication is completed upon removal of excess matrix material (Fig. 1g). A more detailed description of this multi-step assembly process is provided in Extended Data Fig. 1.

By combining micro-moulding with EMB3D printing, we rapidly patterned the required mesofluidic networks by extruding a fugitive ink, which is subsequently removed via auto-evacuation, through a fine nozzle that is embedded within the uncured elastomer matrix. To self-heal crevices that form within the 'body' matrix as the nozzle is translated during the printing process, we created a new elastomeric material containing fumed silica nanoparticles that exhibits thixotropic behaviour[26] (Extended Data Fig. 2a). When completely restructured or at rest, this matrix behaves like a Herschel–Bulkley fluid; that is, it exhibits both shear-thinning behaviour (Extended Data Fig. 2b) and a shear yield stress (Extended Data Fig. 2c). These properties ensure that the extruded inks remain in place within the matrix[13,14]. However, upon yielding, the body matrix readily flows (Extended Data Fig. 2c) into any crevices formed. The body matrix restructures with time, ultimately recovering its original viscoelasticity (Extended Data Fig. 3), which ensures that EMB3D printing can be repeated later in the same matrix region. We also created a 'fuel reservoir' elastomeric matrix, into which

fuel reservoir channels are printed. Both the body and fuel reservoir matrices are cross-linked within the mould after printing is completed.

To create the fuel reservoirs, catalytic reaction chambers, actuator networks and vent orifices, two hydrogel-based inks (fugitive and catalytic) are EMB3D printed within the moulded matrix materials (Fig. 2a). These printed features are interfaced with each other as well as with the soft controller through the use of 'fugitive plugs' introduced at the inlets of the controller before filling the mould with the matrix materials. The fugitive ink is composed of an aqueous, poly(ethylene oxide)-b-poly(propylene oxide)-b-poly(ethylene oxide) triblock copolymer (Pluronic F127) gel[13,27]. The catalytic ink contains platinum particles (Supplementary Video 2) suspended in a mixture of Pluronic F127-diacrylate (F127-DA) and poly(ethylene glycol) diacrylate (PEG-DA) that is photo-cross-linked after printing. The rheological properties of both inks are specifically tailored for EMB3D printing[13,14] (Fig. 2b, Extended Data Fig. 4). The printed features produced from both inks can be changed 'on-the-fly' by varying the print speed (Fig. 2c). Typically, this fugitive ink must be removed or evacuated after printing to yield open channels[13,27]. However, we find that fugitive ink composed of pure Pluronic F127 can be auto-evacuated by heating the printed features within the cross-linked, silicone-based matrices at 90 °C (ref. 28; Fig. 2d, Extended Data Fig. 5). As water evaporation
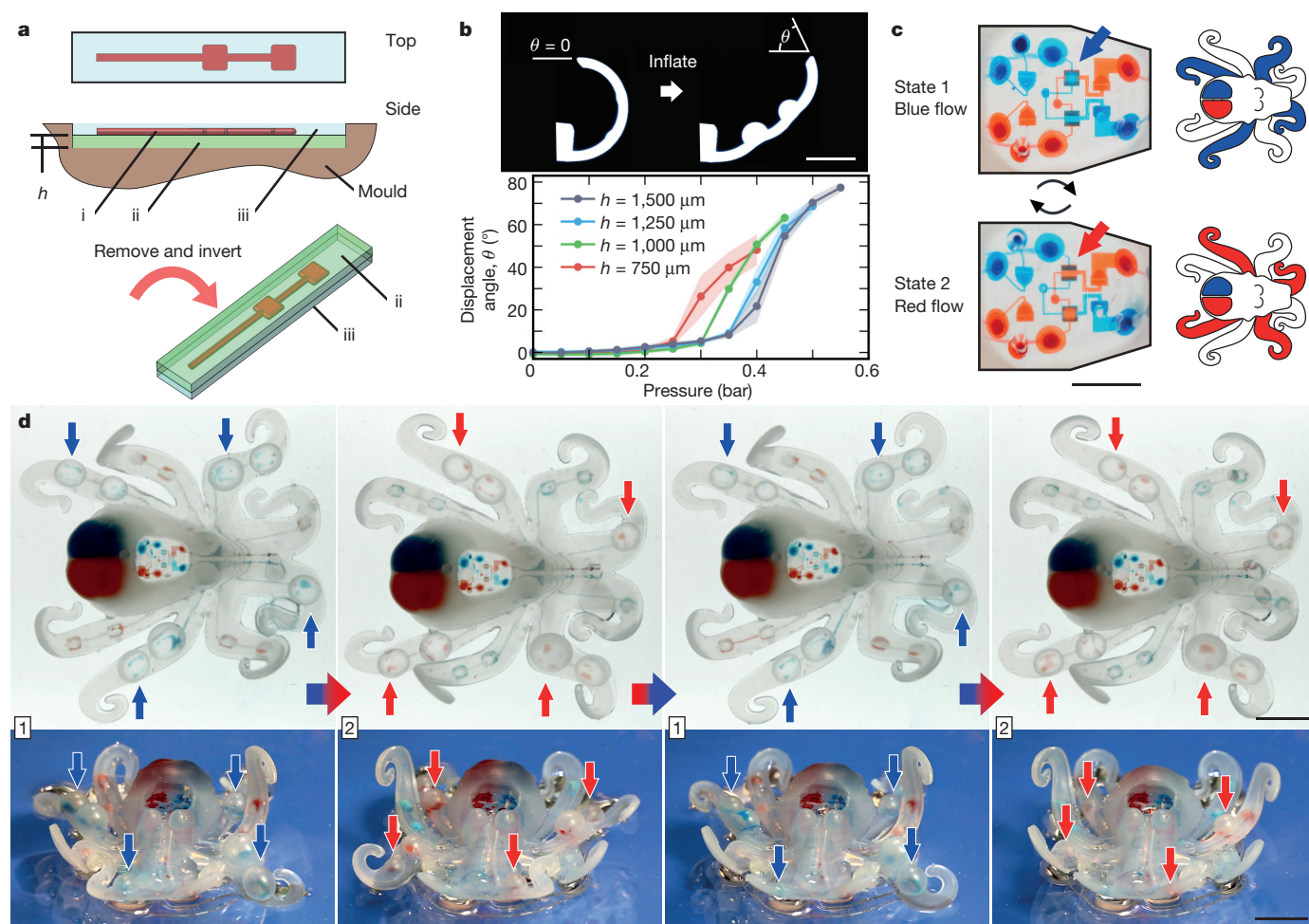

Figure 4 | Octobot actuation. a, Two-bladder actuator design in which traces (i) are printed in contact with the hyperelastic layer (ii) inside the body matrix material (iii) and differences in modulus result in bending upon inflation. The thickness, h, of the hyperelastic layer is modified to change the characteristics of the actuator. In this example, the body matrix material (iii) has a height of 800 μm. **b**, Top, the actuator tip angle, θ, changes upon inflation. Scale bar, 10 mm. Bottom, mean displacement angle, θ, taken from three representative actuators during five inflation

cycles as a function of inflation pressure, for varying hyperelastic layer heights, h (in μm). Error bars, denoted by the shaded regions, indicate the 95% confidence interval. **c**, The oscillator of the soft controller causes an octobot to alternate between blue and red actuation states. The monopropellant fuel is dyed to show states. Scale bar, 5 mm. **d**, Stills from top-down (top; Supplementary Video 5) and face-on (bottom; Supplementary Video 6) operation videos show an octobot autonomously alternating between blue ('1') and red ('2') actuation states. Scale bars, 10 mm.

ensues, the triblock copolymer species either form a thin coating at the matrix-open channel interface or may partially diffuse into the matrix. The fugitive plugs within the inlets of the soft controller also undergo this auto-evacuation process, facilitating connectivity between the microfluidic logic and all printed mesofluidic components (Extended Data Fig. 6). By contrast, the catalytic ink is cross-linked in place after printing, yielding a platinum-laden plug within the matrix (Fig. 2e).

To achieve the desired autonomous function, we incorporated a soft, microfluidic controller within the octobot (Fig. 3a). The control system is roughly divided into four sections: upstream (liquid fuel storage), oscillator (liquid fuel regulation), reaction chamber (decomposition into pressurized gas) and downstream (gas distribution for actuation and venting). Upstream, 0.5 ml of fuel is infused via a syringe pump into each of two fuel reservoirs printed into the hyperelastic matrix. Upstream check valves in the soft controller prevent fuel from flowing back out the fuel inlets. The fuel reservoirs expand elastically to a pressure of approximately 50 kPa, forcing fuel into the oscillator. The oscillator includes a system of pinch and check valves based on prior designs[11], which convert pressurized fuel inflow into alternating fuel outflow. With one channel temporarily occluded, fuel from the other channel flows from the outlets of the soft controller into the platinum-laden reaction chambers, where it rapidly decomposes. The resulting pressurized gas, which is prevented from returning to the soft controller via downstream check valves, flows into one of the downstream mesofluidic networks consisting of four actuators and one orifice. The supplied pressure deflects the actuators and exhausts to atmosphere through the vent orifice. Therefore, for robust actuation and timely venting, a balance must be reached between supply gas flow, actuation pressure and exhaust rate. These subcomponents operate on the basis of the interaction and timing of the local pressures, which is conceptually similar to an electrical oscillator (Fig. 3b). Upon successful venting, the fuel flow into one reaction chamber stops and flow to the other begins, initiating a similar sequence in the other downstream catalytic chamber and actuator network (Fig. 3c).

To provide an on-board power source, we use 50 wt% aqueous hydrogen peroxide as the fuel, owing to its high energy density ($1.44 \, \mathrm{kJ \, g^{-1}}$ as compared to $0.1-0.2 \, \mathrm{kJ \, g^{-1}}$ for batteries) and its benign decomposition by-products. As the fuel decomposes in the presence of the platinum catalyst, the following reaction occurs: $2H_2O_2 \, (l) \rightarrow 2H_2O \, (l, g) + O_2 \, (g)$. This reaction results in volumetric expansion by a factor of approximately 240 (at ambient pressure)[12]. At our operating pressure of 50 kPa, an expansion to 160 times the original volume is expected. Although higher fuel concentrations would provide increased expansion and energy density, concentrations above 50 wt% drastically increase the decomposition temperature, resulting in combustion within the printed catalytic reaction chambers (Supplementary Videos 3 and 4). Because this monopropellant liquid fuel can be handled in small volumes and decomposes at the point of use, we can use microfluidic logic to directly handle the fuel, eliminating the need for external valves[7] to control gas at high pressure and flow rate.

The geometry of the microfluidic soft controller is designed to operate at a fuel flow rate of about $40 \, \mathrm{\mu l \, min^{-1}}$, thereby yielding pressurized gas at a rate of about $6.4 \, \mathrm{ml \, min^{-1}}$ (ref. 11). Under these operating conditions, the theoretical run time of 12.5 min could be achieved using a system with a fuel capacity of 1 ml. The actuators, which consist of printed bladders in contact with a lower-modulus, hyperelastic elastomer layer (Fig. 4a), are designed to inflate asymmetrically to generate angular displacement. Their maximum working pressure and displacement are tuned on the basis of the thickness of the hyperelastic layer (Fig. 4b, Extended Data Fig. 7). If this layer is too thin, then it ruptures prematurely. However, the working pressure increases with thickness. As a compromise, we selected a layer thickness of $1{,}000 \, \mathrm{\mu m}$ because it affords consistent performance at the lowest working pressure. In parallel with the actuators, we tailored the diameter of the vent orifices by modulating print speed. Orifices roughly $75 \, \mathrm{\mu m}$ in width allowed proper actuator displacement with timely subsequent venting.

The ability to rapidly pattern and adjust the geometry of these features on-the-fly via EMB3D printing allowed us to iterate through more than 30 designs and nearly 300 octobots to converge on an appropriate system-level architecture.

Through this iterative process, we created octobots with embedded components that work together in concert to alternate between the red and blue actuation states shown in Fig. 4c. The resulting octobots operated autonomously (Fig. 4d, Extended Data Fig. 8, Supplementary Videos 5 and 6), cycling between actuation states for four to eight minutes. Although this is less than the predicted theoretical run time, the soft controller alternates actuation states as expected. We believe that downstream impedances arising from decomposition–actuation–venting cycles, as well as the decreasing flow rate of fuel into the soft controller with time, are responsible for the departure from theoretical performance[11]. These issues can be addressed by integrating more sophisticated microfluidic circuits, such as universal logic gates, or components with 'gain' that enable advanced control schemes (see Methods for an extended discussion).

We have demonstrated the untethered operation of a robot composed solely of soft materials. The coupling of monopropellant fuels and microfluidic logic allowed us to power, control and realize autonomous operation of these pneumatically actuated systems. Through our hybrid assembly approach, we both constructed the robot body and embedded the necessary components for fuel storage, catalytic decomposition and actuation to enable system-level function in a rapid manner. The octobot is a minimal system designed to demonstrate our integrated design and fabrication strategy, which may serve as a foundation for a new generation of completely soft, autonomous robots.

1. Rus, D. & Tolley, M. T. Design, fabrication and control of soft robots. *Nature* **521,** 467–475 (2015).
2. Wang, L. & Iida, F. Deformation in soft-matter robotics: a categorization and quantitative characterization. *IEEE Robot. Autom. Mag.* **22,** 125–139 (2015).
3. Shepherd, R. F. *et al.* Multigait soft robot. *Proc. Natl Acad. Sci. USA* **108,** 20400–20403 (2011).
4. Onal, C. D., Chen, X., Whitesides, G. M. & Rus, D. Soft mobile robots with on-board chemical pressure generation. *In 15th International Symposium on Robotics Research (ISRR 2011)* 1–16 (2011).
5. Lin, H.-T., Leisk, G. G. & Trimmer, B. GoQBot: a caterpillar-inspired soft-bodied rolling robot. *Bioinspir. Biomim.* **6,** 026007 (2011).
6. Mosadegh, B. *et al.* Pneumatic networks for soft robotics that actuate rapidly. *Adv. Funct. Mater.* **24,** 2163–2170 (2014).
7. Tolley, M. T. *et al.* A resilient, untethered soft robot. *Soft Robot.* **1,** 213–223 (2014).
8. Marchese, A. D., Onal, C. D. & Rus, D. Autonomous soft robotic fish capable of escape maneuvers using fluidic elastomer actuators. *Soft Robot.* **1,** 75–87 (2014).
9. Bartlett, N. W. *et al.* A 3D-printed, functionally graded soft robot powered by combustion. *Science* **349,** 161–165 (2015).
10. Peele, B. N., Wallin, T. J., Zhao, H. & Shepherd, R. F. 3D printing antagonistic systems of artificial muscle using projection stereolithography. *Bioinspir. Biomim.* **10,** 055003 (2015).
11. Mosadegh, B. *et al.* Integrated elastomeric components for autonomous regulation of sequential and oscillatory flow switching in microfluidic devices. *Nat. Phys.* **6,** 433–437 (2010).
12. Wehner, M. *et al.* Pneumatic energy sources for autonomous and wearable soft robotics. *Soft Robot.* **1,** 263–274 (2014).
13. Wu, W., Deconinck, A. & Lewis, J. A. Omnidirectional printing of 3D microvascular networks. *Adv. Mater.* **23,** H178–H183 (2011).
14. Muth, J. T. *et al.* Embedded 3D printing of strain sensors within highly stretchable elastomers. *Adv. Mater.* **26,** 6307–6312 (2014).
15. Palleau, E., Morales, D., Dickey, M. D. & Velev, O. D. Reversible patterning and actuation of hydrogels by electrically assisted ionoprinting. *Nat. Commun.* **4,** 2257 (2013).
16. Ionov, L. Biomimetic hydrogel-based actuating systems. *Adv. Funct. Mater.* **23,** 4555–4570 (2013).
17. Anderson, I. A., Gisby, T. A., McKay, T. G., O'Brien, B. M. & Calius, E. P. Multi-functional dielectric elastomer artificial muscles for soft and smart machines. *J. Appl. Phys.* **112,** 041101 (2012).
18. Brown, E. *et al.* Universal robotic gripper based on the jamming of granular material. *Proc. Natl Acad. Sci. USA* **107,** 18809–18814 (2010).

19. Suzumori, K. Elastic materials producing compliant robots. *Robot. Auton. Syst.* **18,** 135–140 (1996).
20. Shepherd, R. F., Stokes, A. A., Nunes, R. M. D. & Whitesides, G. M. Soft machines that are resistant to puncture and that self seal. *Adv. Mater.* **25,** 6709–6713 (2013).
21. Suzumori, K., Koga, A., Kondo, F. & Haneda, R. Integrated flexible microactuator systems. *Robotica* **14,** 493–498 (1996).
22. Gorissen, B., De Volder, M., De Greef, A. & Reynaerts, D. Theoretical and experimental analysis of pneumatic balloon microactuators. *Sens. Actuat. A* **168,** 58–65 (2011).
23. Shepherd, R. F. *et al.* Using explosions to power a soft robot. *Angew. Chem. Int. Ed.* **52,** 2892–2896 (2013).
24. Whitesides, G. M. What comes next? *Lab Chip* **11,** 191–193 (2011).
25. Mosadegh, B., Tavana, H., Lesher-Perez, S. C. & Takayama, S. High-density fabrication of normally closed microfluidic valves by patterned deactivation of oxidized polydimethylsiloxane. *Lab Chip* **11,** 738–742 (2011).
26. Barnes, H. A. Thixotropy—a review. *J. Non-Newton. Fluid Mech.* **70,** 1–33 (1997).
27. Kolesky, D. B. *et al.* 3D bioprinting of vascularized, heterogeneous cell-laden tissue constructs. *Adv. Mater.* **26,** 3124–3130 (2014).
28. Randall, G. C. & Doyle, P. S. Permeation-driven flow in poly(dimethylsiloxane) microfluidic devices. *Proc. Natl Acad. Sci. USA* **102,** 10813–10818 (2005).

METHODS

Soft controller fabrication. Soft controllers are fabricated from Sylgard 184 PDMS (Dow Corning Corp.) using soft lithography moulding and bonding techniques. First, a mould was fabricated on a silicon wafer using SU-8 negative photoresist (Microchem Corp.). SU-8 3050 photoresist was used to achieve 100-μm film thickness. Baking, exposing and developing steps were performed in accordance with product specifications in the product datasheet. The completed wafer is placed in a Petri dish to form a competed mould assembly.

Soft controllers consist of an upper mould, a lower mould and an intermediate thin film. The upper and lower moulds are made on one wafer to ease fabrication. PDMS is poured into the mould assembly to a height of 1 mm. Separately, PDMS is spin-coated onto a wafer at 1,500 r.p.m. for 60 s for a film thickness of 35 μm. After curing at 90 °C for 20 min, PDMS forms are removed from the moulds and holes are punched at all inlets and outlets. The upper layer is bonded to the wafer-adhered thin film after exposing to oxygen plasma at 35 W for 20 s in a Deiner Pico plasma system (Deiner Electronic GmbH). Holes are punched in the thin film, masks are placed as described in ref. 25, and the lower layer is bonded to the thin film using the plasma recipe above.

Ink and matrix materials. Two inks—a 'fugitive ink' and a 'catalytic ink'—are formulated for EMB3D printing. The fugitive ink is prepared by adding 27 wt% gel of Pluronic F127 to ice-cold, deionized, ultra-filtrated (DIUF) water, followed by mixing in a planetary mixer for 5 min at 2,000 r.p.m., and storing at 4 °C. The fugitive ink is not used until the Pluronic F127 completely dissolves in solution. The ink is prepared for printing by loading the solution at 4 °C in a 3-cm^3 syringe barrel (EFD Nordson) and centrifuged at 3,000 r.p.m. for 5 min to degas. For EMB3D printing, the barrel of the fugitive ink is fitted with a stainless steel nozzle (0.15-mm inner diameter; EFD Nordson).

The catalytic ink is prepared by first synthesizing and then dissolving a diacrylated Pluronic (F127-DA) at 30 wt% concentration with a solution of Irgacure 2959 (at 0.5 wt%, BASF) in DIUF water at 4 °C. The F127-DA is synthesized under an inert nitrogen atmosphere by first adding 400 ml of dry toluene (Sigma-Aldrich Co.) to a three-neck flask fixed to a condenser with circulating cold water and magnetically stirred at 300 r.p.m. 70 g of Pluronic F127 (Sigma-Aldrich Co.) is then dissolved in the toluene after heating the solvent to 60 °C. After the solution is allowed to cool to room temperature, triethylamine (5.6 g, Sigma-Aldrich Co.) is added to the solution, followed by the drop-wise addition of acryloyl chloride (5 g, Sigma-Aldrich Co.) with continued stirring, both at a molar ratio of 10:1 with the Pluronic F127. The reaction mixture is stirred overnight and maintained in the inert atmosphere. The diacrylated Pluronic F127 (F127-DA) product is then filtered from the yellow triethylammonium hydrochloride by-product and precipitated from the filtered solution with hexane (Sigma-Aldrich Co.) at a 1:1 volume ratio. The F127-DA is obtained through a second filtration step and allowed to dry in a chemical hood for at least 24 h. This protocol is adapted from ref. 13. For each gram of this base F127-DA mixture, 100 mg of PEG-DA is added, and this solution is mixed in a planetary mixer for 1 min at 2,000 r.p.m. and degassed for 3 min at 2,200 r.p.m. This mixture is then stored in the dark at 4 °C. Finally, 5 w/w% Pt black (Sigma-Aldrich Co.) is added to this base solution at 4 °C and mixed in a planetary mixer for 5 min at 2,000 r.p.m. The Pt-filled F127-DA physically gels during mixing, facilitating loading into a UV-blocking 3-cm^3 syringe barrel (EFD Nordson) for printing. This catalytic ink is freshly prepared for each print session, as the Pt black slowly cross-links the acrylate moieties present in the ink. After EMB3D printing, the catalytic ink is cross-linked for 15 min at 18 mW cm^{-2} under a UV source (Omnicure EXFO). For EMB3D printing, the syringe barrel housing this ink is fitted with a stainless steel nozzle (0.33-mm inner diameter; EFD Nordson).

Two matrix materials are developed for fabricating fully soft robots. The first matrix, referred to as the 'body matrix', is prepared by blending two silicone-based materials: Sylgard 184 and SE 1700 (Dow Corning Corp.). SE 1700 is a silicone elastomer paste that contains fumed silica nanoparticles. Sylgard 184 PDMS is used to dilute SE 1700 to achieve the optimal rheological response for embedded 3D printing. After exploring several blends, we found that the optimal body matrix is composed of a 1:1 mass ratio of SE 1700 (4:1 ratio of base to hardener) and Sylgard 184 (10:1 ratio of base to hardener). This matrix is prepared by mixing the blend in a planetary mixer at 2,000 r.p.m. for 3 min with degassing at 2,200 r.p.m. for 2 min. The second matrix, referred to as the 'fuel reservoir matrix', is prepared by mixing Part A Ecoflex 00-30 to Part B Ecoflex 00-30 (with 1.2 w/w% Slo-Jo Platinum Silicone Cure Retarder and 1.2 w/w% Thivex, Smooth-On Inc.) in a 1:1 ratio. The matrix is prepared in a planetary mixer at 2,000 r.p.m. for 1.5 min with degassing at 2,200 r.p.m. for 1 min.

Last, the 'fugitive plug' material used to prevent ingress of the body matrix material into the soft controller is prepared before printing by first synthesizing and then mixing a diacrylated Pluronic material (F127-DA) (at 30 wt% in a 0.5 wt% solution of Irgacure 2959 in deionized water) with F127 (at 30 wt% in deionized water) at a mass ratio of 1:4. The fugitive plug is stored in the dark at 4 °C in a syringe. When used, the fugitive plug material is allowed to physically gel before it is cross-linked for 3 min at 6 mW cm^{-2} under a UV source.

Rheological characterization. All rheological measurements are carried out using a controlled-stress rheometer (DHR-3, TA Instruments) equipped with a 40-mm-diameter, 2° cone and plate geometry. In all experiments, the fugitive and catalytic inks are equilibrated at room temperature for 1 min before testing; the fuel reservoir and body matrix materials are equilibrated for 20 min and 10 min, respectively, to simulate the times at which octobot printing began with each material. Shear storage moduli are measured as a function of shear stress at a frequency of 1 Hz.

The body matrix materials are characterized by both flow sweep and flow ramp tests to determine their rheological response (Extended Data Fig. 2). In addition, three-phase modulus recovery tests are carried out to quantify the recovery time of the body matrix stiffness after applying a shear stress that exceeds the equilibrium yield stress, $\tau_{y,0}$ (Extended Data Fig. 3). In the first set of experiments, flow sweeps from low (10^{-2} s^{-1}) to high (10^2 s^{-1}) shear rates are carried out immediately followed by flow ramps from high to low shear rates. In the second set of experiments, shear storage (G') and loss (G'') moduli are measured during three phases of applied shear stresses (at 1-Hz frequency): 1 Pa for 3 min; 100 Pa for either 1 s, 10 s or 100 s; and 1 Pa for 30 min. We defined their thixotropic recovery time as the instant $G' = G''$, or when $\tan(\delta) = G''/G' = 1$, where δ is the phase angle.

Actuator characterization. Actuators are printed into special actuator characterization moulds by EMB3D printing and then auto-evacuate. To prepare them for characterization, they are first released from mould assembly and then a 1-mm hole is created with a biopsy punch (Miltex Inc.), which serves as the air inlet. Finally, the actuator is pressurized slightly to ensure inflation. Each actuator design is tested for angular displacement (that is, the actuator is allowed to deflect unconstrained and the total displacement angle is measured) and blocked force (that is, the actuator is constrained from deflection and resultant force is measured; see Extended Data Fig. 7). For each actuator, break-in testing consists of five cycles, in which actuator air pressure is slowly (over about 30 s) ramped up to the pressure set point, then slowly (over about 30 s) ramped down to ambient. Pressure set point for the first cycle is P_0 and the set point for all subsequent cycles is P_1 (Extended Data Table 1). Data acquisition consists of five additional cycles for each actuator, in which air pressure is cycled as above to pressure set point P_1.

To characterize their angular displacement, actuators are plumbed with regulated compressed air and mounted vertically between a matte black background and a Sony NEX3 digital camera for video data acquisition. Actuators are pressurized in cycles as described above, followed by five data-acquisition cycles. As above, the first break-in cycle is to P_0 and all subsequent break-in and data-acquisition cycles are to P_1. Video data are analysed using the ImageJ image analysis platform (NIH.gov) to obtain the bend angle versus pressure for each actuator.

For blocked-force characterization, individual actuators are mounted on a fixed platform beside an Instron model 5544 materials testing frame (Illinois Tool Works Inc.). The actuator is lowered until just above the force sensor portion of the testing frame and the actuator is plumbed with regulated compressed air. Actuators typically behave differently upon the initial few actuations versus subsequent actuations, owing to the Mullins effect[29]. Each actuator therefore receives five break-in cycles before data acquisition. Air pressure and actuator force data are recorded on the Instron testing frame data acquisition system at 100-ms intervals.

Mould fabrication. Octobot moulds are fabricated inside a CNC machined acetal mould equipped with two locating pins to mount the soft controller. Their desired shape is modelled in SolidWorks (Dessault Systemes SOLIDWORKS Corp.). A negative mould is modelled and output in Parasolid format for file transfer. MasterCAM (CNC Software, Inc.) is used to develop all machining tool paths and to export the final G-code for final fabrication. Blanks (12.7 cm × 7.6 cm × 2.54 cm) were cut from black acetal (Delrin) (McMaster Carr). Acetal is used, owing to its dimensional stability, and 2.54-cm-thick stock is chosen to prevent warping during machining and repeated octobot curing cycles. Octobot moulds are produced by CNC milling on a HAAS OM-2A vertical machining centre (HAAS Automation Inc.). 1-mm dowel pins are pressed into drilled holes for controller mounting.

Soft robot assembly. A custom-designed, multi-material 3D printer (ABL 10000, Aerotech Inc.) with four independently z-axis addressable ink reservoirs is used to pattern fugitive and catalytic inks within the octobot matrices[27]. All G-Code for printing is generated from Python-based software (MeCode, developed by J. Minardi). Prior to EMB3D printing, Ecoflex 30 (Smooth-On, Inc.) is first prepared with 1 wt% Slo-Jo and 0.25 wt% Thivex (both with respect to Part A) by mixing in a Thinky planetary mixer for 1.5 min with a 1-min degas cycle. This uncured Ecoflex 30 is cast into the actuator layers of the octobot mould and degassed in a vacuum chamber for 3 min. A glass slide is used to remove excess material and create smooth surfaces that will ultimately become the extensible layers of the actuators. The moulds are then placed in a 90 °C oven for 30 min to cure the Ecoflex, removed, and trimmed of excess material as necessary.

A soft controller is then loaded onto the press-fit pins placed in the printing mould with the polyimide (Kapton) tape still adhered. Registration coordinates and print heights are then taken from the cured Ecoflex layers in the actuators and in all inlets of the soft controller; these are essential for EMB3D printing and provided to the custom print software. The fuel reservoir and body matrix materials are prepared as described previously. While the body matrix material is mixing, the fuel reservoir matrix is deposited in the fuel reservoir region of the printing mould. It is then degassed for 3 min to ensure no trapped gas is present. Excess bubbles in the uncured fuel reservoir matrix are removed with a pipettor. The non-gelled, chilled fugitive plug is then filled throughout the soft controller via injection through the inlets. While the fugitive plug is still in the liquid state, it is briefly degassed in a vacuum chamber. The fugitive plug material is then allowed to physically cross-link, excess gel is scraped from the top of the tape, the tape is removed, and the fugitive plug is photo-cross-linked with a UV source at 6 mW cm^{-2} for 3 min. After the gels are cross-linked, the body matrix is cast within the mould, covering the fuel reservoir matrix and the fugitive plug-filled soft controller and degassed for 1–3 min *in situ*. Again, excess bubbles are removed with a pipettor, excess material is scraped off and away from the mould with a glass slide, and EMB3D printing of the fugitive and catalytic inks begins. After printing, the entire mould is cured at 18 mW cm^{-2} for 15 min to crosslink the catalytic ink. The mould is then transferred to a 90 °C oven, where the matrix materials cross-link. The octobot is removed from the mould and kept at 90 °C for 4 days to facilitate auto-evacuation of the inks.

After auto-evacuation, the octobot is release-cut from the surrounding matrix material using a CO$_2$ laser (Universal Laser Systems) and cleaned with isopropyl alcohol and water. Sylgard 184 PDMS (Dow Corning Corp.) is poured into the open cavity of the octobot above the soft controller to a height of 1.5 mm and cured at 90 °C for 20 min. A 1-mm biopsy punch (Miltex Inc.) is used to punch holes through the newly poured PDMS layer and into the fuel inlets. Dyed water is injected into these holes to inflate the fuel tanks, flow through the system and insure proper bot function. Holes are punched in the downstream vent orifices to allow the water to vent from the system.

The octobot is loaded into an acrylic tank outfitted with a backlight to highlight coloured fuel as it flows through the system. Aqueous hydrogen peroxide (90 wt%, HTP grade, Peroxychem) is diluted to 50 wt% and samples dyed red and blue are filled into two syringes prepared with this liquid fuel mixture. The syringes are loaded onto a syringe pump, and connected to the octobot via 1-mm-diameter silicone rubber tubing. Water is flowed into the acrylic tank to wash away dye in the octobot exhaust stream and drained into a nearby sink. The syringe pump flows fuel at a rate of 3 ml min^{-1} (each syringe) into the octobot for 10 s. The silicone rubber tubing is removed with tweezers from the octobot, which is allowed to operate untethered. The octobot alternates actuation until fuel pressure is insufficient to switch the oscillator and alternating actuation ceases.

Imaging and videography. Photographs and supporting videos are acquired with a digital SLR camera (Canon EOS 5D Mark II, Canon USA Inc.) and a 4K video (Blackmagic Production 4K, Blackmagic Design). Photos are cropped using Inkscape vector graphics editor (http://www.inkscape.org) and video sequences are clipped from raw footage and exported using iMovie (Apple Corp.; titles are added using Premiere Pro, Adobe Systems, Inc.). All print parameter measurements and images of EMB3D printed features in octobots are taken with a digital zoom microscope (VHX-2000, Keyence). Their mean values and standard deviations are determined from three samples printed at each print speed of interest.

Considerations for future microfluidic controllers, logic and actuation. The octobot represents a minimal soft robotic system that demonstrates our integrated design and fabrication strategy. In our self-contained microfluidic controllers, system scaling is limited by fuel flow rate, on-board fuel supply, downstream decomposition/expansion and actuation-network design. At 50% concentration by weight, 1 g of aqueous hydrogen peroxide expands to approximately 200 ml of gas under ambient pressure and temperature conditions[12]. Our oscillator is designed to operate at 40 μl min^{-1} per channel (80 μl min^{-1} total), and our actuators inflate with approximately 0.2 ml at 50 kPa, the equivalent of 0.3 ml at ambient pressure. Hence, with each channel inflating four actuators, our current design has a theoretical maximum oscillation rate of 5.5 switches per minute. Although the controller and actuators could be redesigned for increased performance, any system scaling would require careful balancing of fuel supply, flow rate and actuator requirements. Alternative actuator designs are possible (see Extended Data Fig. 7), but our current actuators produce 0.04 N; therefore, two actuators would theoretically be sufficient to lift the 7-g robot.

On the basis of these demonstrated capabilities, we anticipate that more sophisticated microfluidic control systems and logic devices could be readily incorporated within these printed and moulded robots. For example, fluidic versions of electric logic gates have been reported, including NAND/NOR, AND/OR and XOR/XNOR[30–32], and flip-flops and gain valves[33–35]. These complex systems are based on well-established, electrical design rules. Implementation of these systems would enable more complex actuation strategies, such as multi-degree-of-freedom actuators in which planned limb motion would prescribe a true gait with aerial and ground phases to lift and propel the soft robot. Alternatively, actuators could be designed to take advantage of material elasticity, in which actuation performs flexion and abduction, and passive limb elasticity provides extension and adduction. One could even envision an actuation strategy in which pneumatic channels act as sensors, providing true closed-loop feedback to the controller.

29. Mullins, L. Softening of rubber by deformation. *Rubber Chem. Technol.* **42,** 339–362 (1969).
30. Jensen, E. C., Grover, W. H. & Mathies, R. A. Micropneumatic digital logic structures for integrated microdevice computation and control. *J. Microelectromech. Syst.* **16,** 1378–1385 (2007).
31. Rhee, M. & Burns, M. A. Microfluidic pneumatic logic circuits and digital pneumatic microprocessors for integrated microfluidic systems. *Lab Chip* **9,** 3131–3143 (2009).
32. Toepke, M. W., Abhyankar, V. V. & Beebe, D. J. Microfluidic logic gates and timers. *Lab Chip* **7,** 1449–1453 (2007).
33. Groisman, A., Enzelberger, M. & Quake, S. R. Microfluidic memory and control devices. *Science* **300,** 955–958 (2003).
34. Weaver, J. A., Melin, J., Stark, D., Quake, S. R. & Horowitz, M. A. Static control logic for microfluidic devices using pressure-gain valves. *Nat. Phys.* **6,** 218–223 (2010).
35. Prakash, M. & Gershenfeld, N. Microfluidic bubble logic. *Science* **315,** 832–835 (2007).
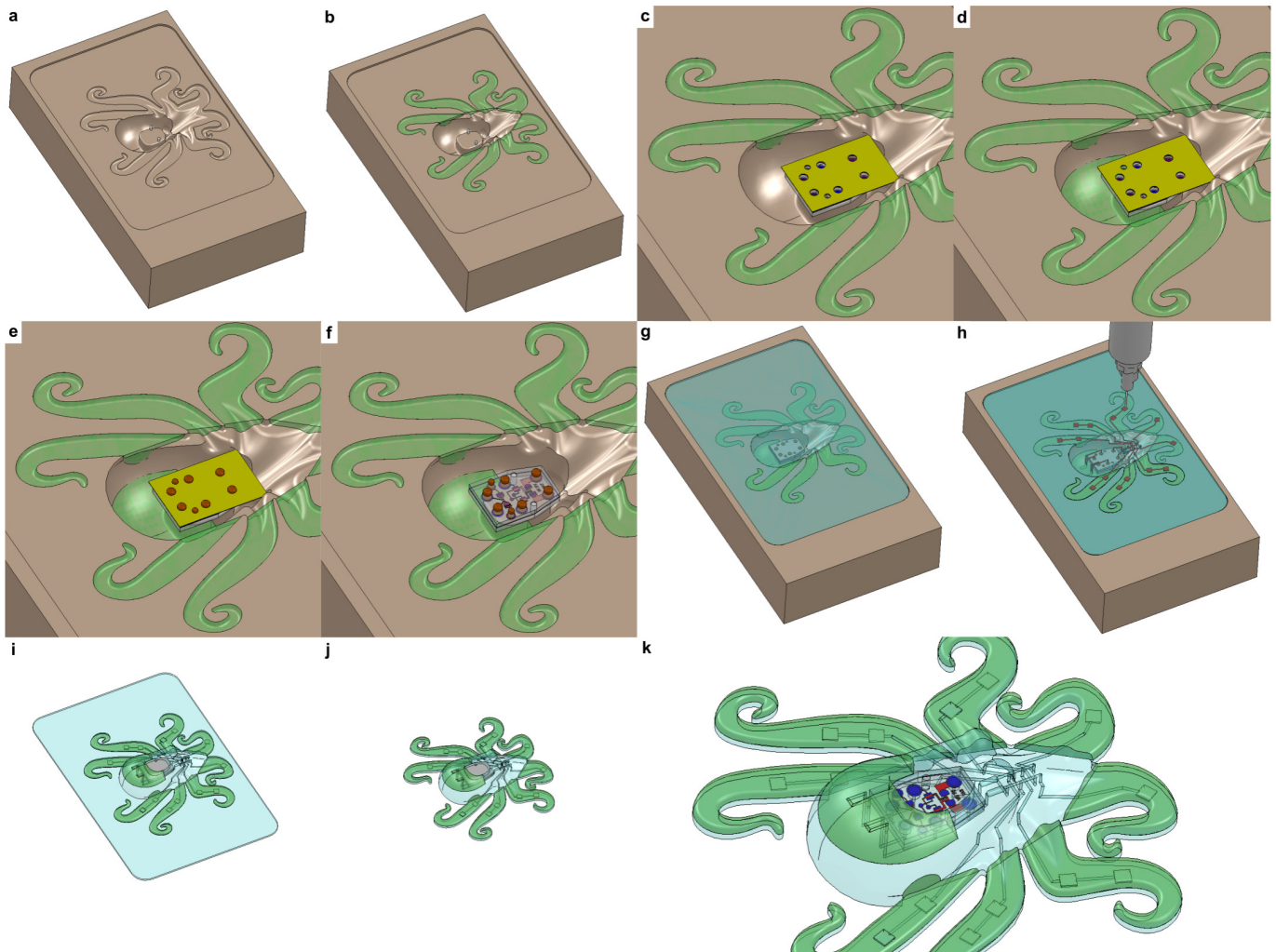
Extended Data Figure 1 | EMB3D printing of an octobot. a, An EMB3D printing mould is machined from acetal. **b**, The hyperelastic layers needed for actuation are cast and cross-linked in the actuator regions of the mould. **c**, A soft controller protected with a polyimide tape mask is loaded onto the pins of the EMB3D printing mould. **d**, The fuel reservoir matrix material is carefully loaded into the fuel reservoir area of the mould and degassed under vacuum. **e**, Liquefied fugitive plug material is manually loaded into the soft controller via the inlets and briefly degassed. **f**, The protective tape is removed after the fugitive plug material physically gels, and the fugitive plug is photo-cross-linked. **g**, The body matrix material is cast into the mould and degassed. **h**, Any excess body matrix material is removed with a squeegee step, EMB3D printing begins, and the entire mould and EMB3D-printed materials are placed in a 90 °C oven to cross-link. **i**, After 2 h, the cross-linked octobot is removed from its mould and kept at 90 °C for a total of 4 days to ensure complete auto-evacuation of the aqueous fugitive inks. **j**, Before operation, excess body matrix material is removed via laser cutting. **k**, The final octobot, shown here in a close-up view, is prepared for operation.
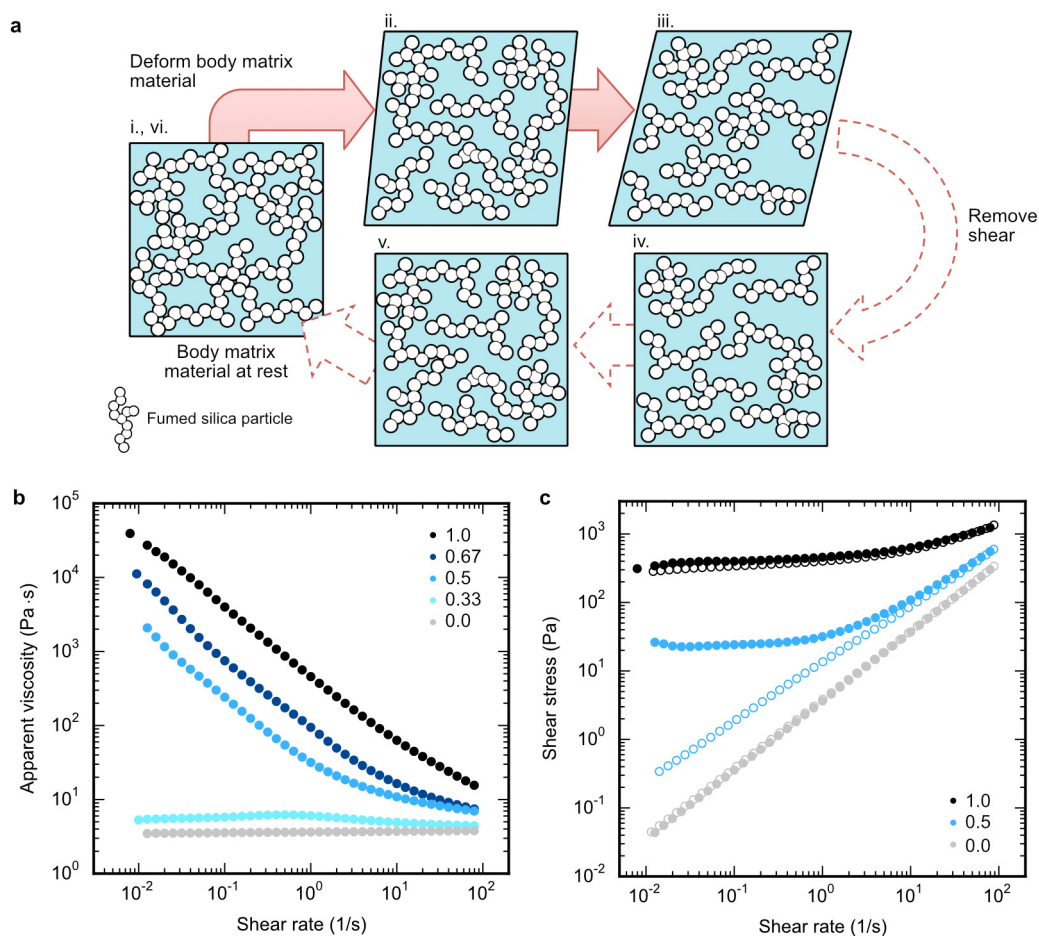
Extended Data Figure 2 | Rheological properties of the body matrix.
a, Schematic illustration of the behaviour of the body matrix during the EMB3D printing process. (i) When the body matrix is at rest, the fumed silica fillers within the silicone material form a percolated network, giving rise to its equilibrium, at-rest shear yield stress, $\tau_{y,0}$. (ii) As the nozzle travels through the matrix during EMB3D printing, the matrix is yielded and the percolated filler network is disrupted, decreasing the apparent yield stress of the matrix material, $\tau_{y,t}$. (iii) Sufficient deformation can completely disrupt the fumed silica microstructure and completely eliminate the yield stress of the matrix material ($\tau_{y,t} \rightarrow 0$ Pa). (iv) The fumed silica network does not immediately recover when it returns to a quiescent state. (v) Over time, the network slowly restructures to (vi) its equilibrium microstructure, and $\tau_{y,t} \rightarrow \tau_{y,0}$. **b, c**, Log–log plots of

apparent viscosity (**b**) and corresponding shear stress (**c**) versus shear rate for various PDMS matrix formulations, which are prepared by blending Sylgard 184 (10:1 ratio of base to hardener) and SE 1700 (4:1 ratio of base to hardener) at various mass fractions. The formulations are listed by the weight ratio of SE 1700 used (0.0, 0.33, 0.5, 0.67 and 1.0). Closed and open circles in **c** represent measurements taken during the flow sweep and flow ramps of the thixotropic loop studies, respectively. The final body matrix, formulated from the 50 wt% SE 1700 blend, shows clear thixotropic behaviour and a substantial decrease in yield stress upon yielding. Blends with higher concentrations of filler particles show diminished thixotropic behaviour, and the yield stress is not eliminated during nozzle translation. Consequently, crevices or air pockets form during printing, with matrix materials possessing higher concentrations of fumed silica.
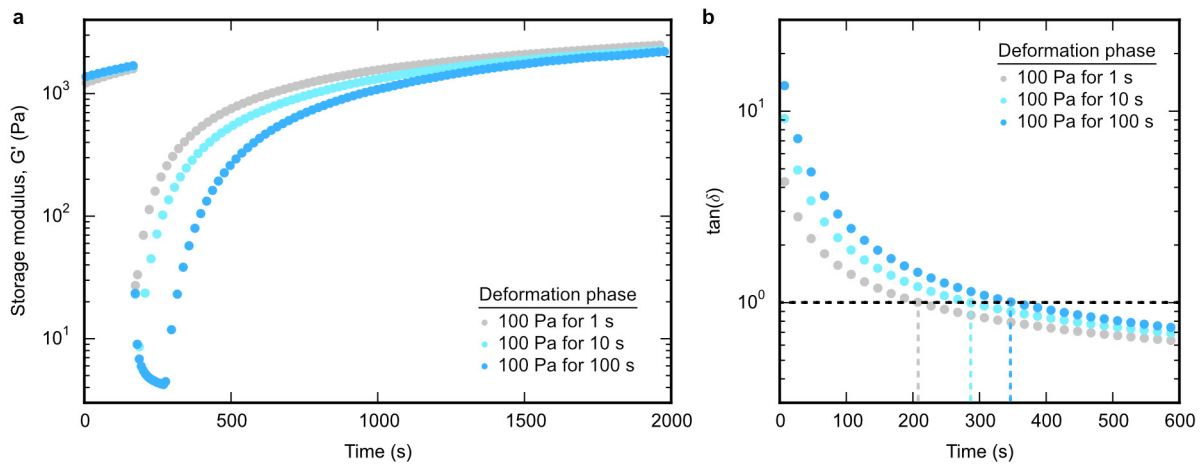
**Extended Data Figure 3 | Storage modulus recovery of the body matrix after yielding. a**, A plot of storage modulus (G') as a function of time illustrates how the modulus of the body matrix recovers during three-phase thixotropy tests. After a probe phase, a shear stress of 100 Pa is applied for varying times during a deformation phase, resulting in temporary fluidization of the matrix material. During the recovery phase, the modulus increases over time. **b**, The ratio of the loss modulus to the storage modulus, $G''/G' = \tan(\delta)$, is plotted as a function time for each of the recovery phases measured in **a**. The onset of recovery of the yield stress of the body matrix material—and the onset of fumed silica filler percolation in a recovering matrix material—is assumed to be the moment $G' = G''$ or $\tan(\delta) = 1$ (horizontal dashed line). Therefore, the 'recovery time' of the body matrix material (indicated by the vertical dashed lines) is approximately the time at which $\tan(\delta) = 1$ after deformation. Because the momentary deformation incurred by nozzle translation through a discrete volume of matrix material during EMB3D printing happens within a time period shorter than 1 s and with a magnitude of less than 100 Pa, the thixotropic recovery time of the body matrix material is less than 200 s—the approximate time it takes the body matrix to recover after being sheared by a 100-Pa stress for 1 s.
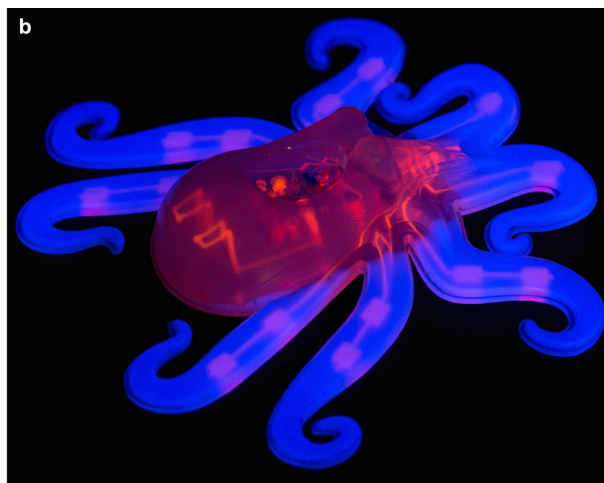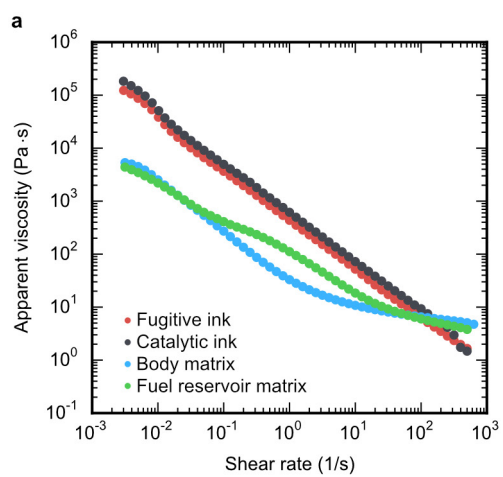
Extended Data Figure 4 | Rheological and printing behaviour of inks and matrix materials. a, A log–log plot of apparent viscosity as a function of shear rate for the fugitive ink (red), catalytic ink (black), body matrix material (blue) and fuel reservoir matrix material (green). **b**, An octobot with fluorescently dyed fugitive inks (red, not auto-evacuated) and hyperelastic actuator layers (blue) fabricated by moulding and EMB3D printing.

| t = 0 h | t = 16 h | t = 43 h | t = 69 h |
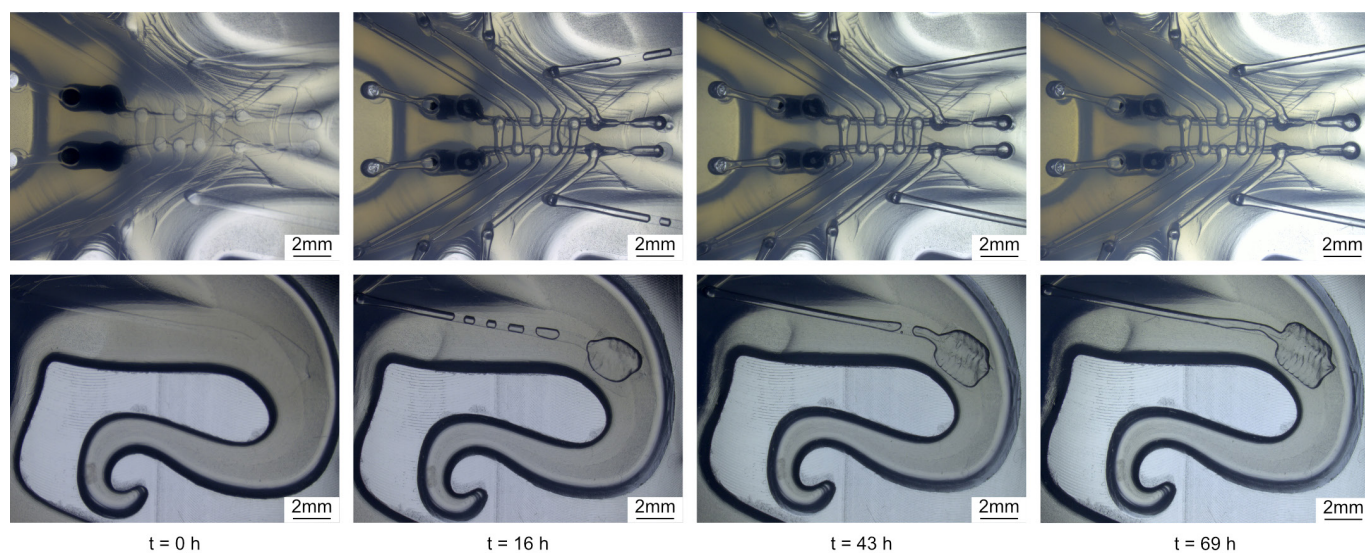
Extended Data Figure 5 | Auto-evacuation of the fugitive and catalytic inks. Photographs of the reaction chambers of an octobot showing the upstream portions of the actuator networks (top) and a one-pad actuator (bottom) at various times, *t*. These photographs reveal the auto-evacuation of the fugitive and catalytic inks, which leaves behind open channels that serve as mesofluidic features.
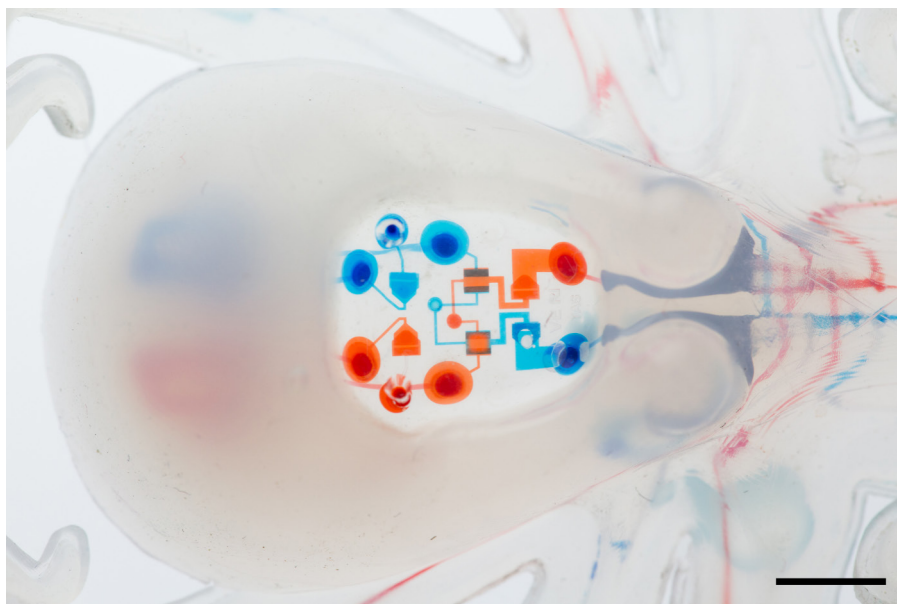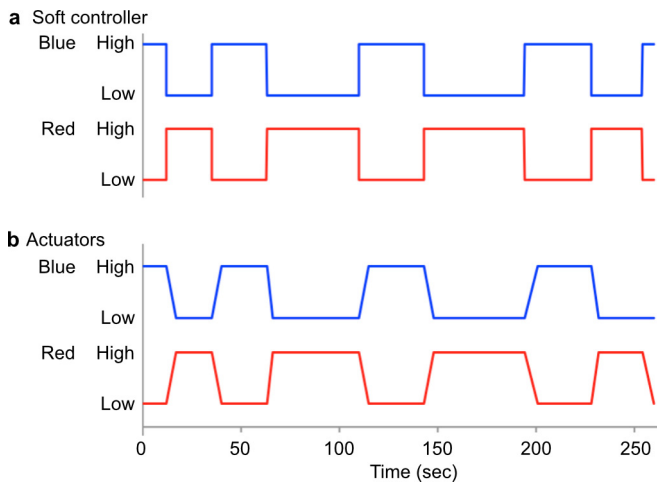
Extended Data Figure 6 | Infilling the soft controller from the fuel inlets. Water (with red or blue dye) is introduced into the fuel reservoir via the fuel inlets. Continuity between the fuel reservoirs, soft controller and downstream EMB3D-printed components is possible because of the fugitive plugs, which auto-evacuate along with the EMB3D-printed inks. Scale bar, 5 mm.
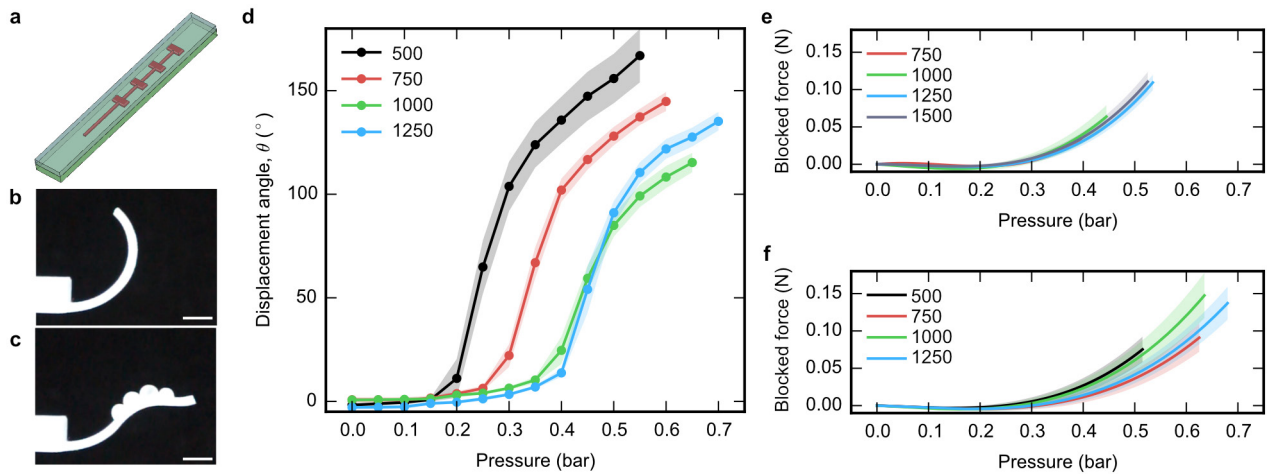
Extended Data Figure 7 | Characterization of EMB3D-printed actuators. a, CAD model of a four-bladder actuator design. Other than bladder number, the design is similar to the actuators illustrated in Fig. 4a. **b**, EMB3D-printed actuator is shown before inflation. **c**, Actuator inflated to working pressure. Scale bars in **b** and **c**, 5 mm. **d**, Pressure versus displacement curves for four-bladder actuators with varying hyperelastic-layer thickness, *h* (see legend; values in micrometres). The data points reported are the mean inflation displacement angles for two representative actuators over five inflation cycles and the shading indicates 95% confidence intervals. **e**, **f**, Blocked force versus pressure curves for two-bladder (**e**) and four-bladder (**f**) actuators of varying hyperelastic-layer thickness, *h* (see legends; values in micrometres). The lines shown are third-degree polynomial fits of data collected from five inflation–deflation cycles of representative actuators. The shaded regions indicate 95% confidence intervals. Detailed procedures for characterizing actuator performance are provided in Methods.

Extended Data Figure 8 | Autonomous switching between actuating states during octobot operation. a, Switching in the soft controller was tracked with time according to the octobot operation recorded in Supplementary Video 5. **b**, The corresponding inflation of actuators associated with the blue and red and actuation states are also reported with time.

Extended Data Table 1 | Break-in and working gauge pressures for printed actuators

Hyperelastic layer thickness (μm)	Two bladder actuators		Four bladder actuators	
	P_0 (Bar)	P_1 (Bar)	P_0 (Bar)	P_1 (Bar)
500	0.35	0.3	0.6	0.55
750	0.4	0.35	0.65	0.6
1000	0.45	0.4	0.7	0.65
1250	0.5	0.45	0.75	0.7
1500	0.55	0.5	0.8	0.75

Before characterizing an actuator, break-in testing consisted of five cycles, in which actuator air pressure is slowly (over about 30 s) ramped up to the pressure set point, then slowly (over about 30 s) ramped down to ambient pressure. The pressure set point for the first cycle is P_0 and the set point for all subsequent cycles is P_1. Data acquisition consists of five additional cycles for each actuator, in which air pressure is cycled as above to pressure set point P_1.